35th Annual International Conference of the IEEE EMBS
Osaka, Japan, 3 - 7 July, 2013

A ROBUST SEMI-AUTOMATIC APPROACH FOR ROI SEGMENTATION IN 3D CT IMAGES

Kongkuo Lu[1], *Zhong Xue*[2], *Stephen T. Wong*[2]

[1] Philips Research North America,Briarcliff Manor, NY; [2] The Methodist Hospital Research Institute, Houston, TX

ABSTRACT

In CT-based clinical applications, segmentation of regions of interest (ROIs) is a preliminary but vital step. The task is, however, quite challenging, especially for 3D objects, because suspicious ROIs are usually soft-tissue structures, which include a various organs and anatomical objects while sharing a small intensity dynamic range in CT images. Furthermore, the ROIs usually vary significantly in size, shape, and boundary conditions. Among considerable efforts contributed to addressing the problem, live wire, also known as intelligent scissors, has been recognized as an efficient and robust tool for dealing with a wide range of 2D ROIs. Such an approach provides full user control during the process while minimizing human interaction to optimally counterbalance automatic and manual approaches. In this work, we improve our previous live-wire-based segmentation of 3D objects and the experiment results show its efficiency and robustness.

Index Terms— Lung cancer, liver cancer, CT, semi-automatic segmentation, live wire

I. INTRODUCTION

CT has been used as a standard image modality for assisting in screening, diagnosis, and treatment of cancers, such as lung and liver. With the development of advanced high-resolution scanners, detailed internal anatomy can be visualized. It is possible to detect the disease in early stages, enable accurate diagnosis, plan and treat the patient with CT guidance, and perform patient follow-ups. In different stages of cancer management, segmentation of regions of interest (ROIs), such as lymph node, tumor, and nodule, is a preliminary but vital step. However, the task is quite challenging because CT is limited in presenting soft-tissue structures, including typical ROIs and various organs. Furthermore, the ROIs may vary significantly in size, shape, boundary condition, etc. Automatic approaches don't require human interaction but they are highly application dependent. Manual methods always work, but they are too time-consuming and cannot guarantee repeatable results.

In the literature, considerable efforts have been contribute to develop semi-automatic methods to counterbalance automatic and manual approaches. Deformable model or level-set-based methods have been successful for many applications. They require an initial setup and then automatically searching for true boundary to optimize relevant cost functions. However, the process will have to start over when the result is not satisfactory. Live wire has been recognized as an efficient and reliable option for segmenting a wide range of 2D ROIs. It converts boundary detection into a graphic search, providing full user control during the segmentation while minimizing human interaction. This approach is extended to 3D by either processing several sectional images from orthogonal planars; or iteratively adjusting boundary initialized using segmentation results from the previous sequential sectional images. In this paper, we re-conduct the 3D segmentation workflow proposed in previous work based on the second scenario[1]. The approach introduce new control parameters and cost features to maximally extract knowledge from previous segmentation and improve segmentation and continuities of a new processed image. The method will be discussed in detail in Section II. Section III will validate the approach and present the results. Section IV concludes the paper.

II. METHOD

In this section, we will first briefly review the paradigm of the 2D live-wire approach and its extension to 3D. Then, we will discribe the new framework in the following subsections.

II-A. 2D Live wire

The basic idea of the original live wire method is to convert the boundary definition problem into a graphic searching. So a cost function is defined to calculate and define the "cost" for connecting a pixel to its adjacent 8 neighborhood pixels. When a control point or seed, s, is selected, the optimal paths from all other pixels in the relevant image area will then be calculated through dynamic programming. During the interaction, the optimal paths from a target location, indicated by the user, will show to suggest a segment candidate. A typical cost function is as follows:

$$c(p,r) = w_Z f_Z(r) + w_G f_G(r) + w_D f_D(p,r) + \{...\} \quad (1)$$

where r is a pixel adjacent to p, $f_Z(r)$ and $f_G(r)$ are Laplacian zero-crossing and gradient magnitude, and $f_{D(p,r)}$ is a gradient-direction cost [2], [3]. The costs are normalized

and reversed if necessary so that pixels along the boundary have small costs. w_x are weights of the corresponding cost and $\sum(w_x) = 1$, and can be adjusted by the user. Additional costs can also be used to improve the segmentation performance[2], [3], [4]. Thus, total cost between a seed s and another pixel, defined as the sum of such cost defined by pixel pairs, (p, r), in between, is used as the path cost. In applications, the user can drive the segmentation process using mouse cursor to define the boundary one segment at a time till a complete segmentation is reached, as demonstrated in Fig.1. Since the user has the full control during the process, 2D live wire is able to deal with almost all kinds of objects though large computation might be necessary for large ROIs.

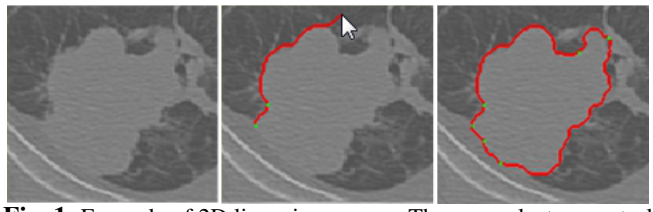

Fig. 1. Example of 2D live wire process. The user selects a control point s, green dot, then a suggested boundary segment will show to link the mouse cursor and s. When a satisfactory segment is achieved, it is confirmed by selecting a new seed. The process is terminated by closing the boundary. The ROI is a tumor located in the right lung.

II-B. Iterative Live Wire

Several approaches have been developed to extend live wire to 3D[5], [6], [7], [4], [1]. One option is to reduce the problem to 2D, instead of a true 3D implementation, to segment the object all relevant parallel 2D sectional images and the 2D results form the 3D segmentation. Iterative live wire (ILW) uses 2D live wire to define a 2D boundary, B, on a selected slice i, then B is projected to slices $i+1$ and $i-1$ as an initial boundary, B_{init}. Several control points, $S = \{s_j\}, j = 1, \cdots, N$, will be selected, to separate B_{init} into N segments evenly (except for segment N). The boundary segments between each pair of s_j, s_{j+1}, $s_{N+1} = s_1$ for defining segment N, will be redefined following live wire paradigm resulting a new boundary segment that is close to the true boundary on current image (except for pixels closed to s_j and s_{j+1}. The boundary will then be adjusted iteratively with different S chosen correspondingly, i.e. choose the middle pixel on segment between s_j and s_{j+1} as new seed for next iteration. When the accumulated cost, C_B, along the boundary does not change or vary slightly from one iteration to the following, $\triangle C_B < c_{min}$, the process ends and the result,B_{i+1}, will be stored and passed to its following slice, B_{i+1} to $i+2$ or B_{i-1} to $i-2$. The process will be performed automatically until stopping conditions are activated. Fig.2 shows an example of ILW segmentation.

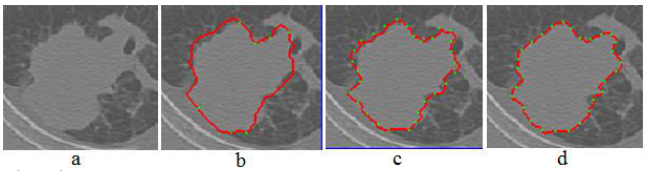

Fig. 2. Iterative live wire process. a. Original image, ROI is as that in Fig.1. b. B_i is projected onto I_{i+1} as B_{init}. B_{init} is close to the true boundary, but not the same. c. Seeds were selected along B_{init} and the boundary is redefined using 2D live wire. d. Iteratively, the boundary candidate is approaching toward the real one and the process stops when minor change of boundary cost is observed between two subsequent iterations.

II-C. Improved Iterative Live Wire

In addition to project B from slice i to $i+1$, to provide a good B_{init}, assuming object boundary does not change dramatically between two subsequent slices (which is true in standard CT images), we can use more information from the previously segmented object area to improve the segmentation result. In this paper, the cost function is formulated as below:

$$\varsigma(p, r) = \mathcal{B}(r)(w_Z f_{Z\circ T}(r) + w_G f_{G\circ T}(r) + w_D f_{D\circ T}(p, r) + w_{\mathcal{P}} f_{\mathcal{P}}(r)) \quad (2)$$

Let I_i be the processed image area on slice i, $i \in [i_{min}, i_{max}]$. i_{min} and i_{max} are slice limits that encompass the ROI and can be set manually or automatically[1]. $\mathcal{B}$ is a characteristic function to apply the geometric data of boundary B_i defined on slice i to slice $i+1$. It can be used either to narrow the search range or as a global weight to local cost. $\mathcal{B}$ reduce computation and improve distinguishing local difference. An example can be:

$$\mathcal{B}(r) = \begin{cases} 1, & \|r - B_{init}\| < R \\ \infty, & \text{otherwise} \end{cases} \quad (3)$$

which is used to mask an local region whose distance to B_{init} is within limit R which is defined manually or automatically based on spatial resolutions of the CT image. $\mathcal{B}$ can also be defined using distance transform. $f_{Z\circ T}(r)$, $f_{G\circ T}(r)$, and $f_{D\circ T}(r)$ are the gradient and gradient direction features calculated based on a transformed image I'_{i+1}, where T is an image transform function that uses anatomical or image features presented by segmented area included by B_i on I_i. T is used to enhance I_{i+1}, to I'_{i+1}, to improve boundary searching. A typical T can be a maximum likelihood (ML) transform. Let O_i be the object area bounded by B_i, and the mean and standard deviation of its pixel intensities are μ_{O_i} and σ_{O_i}. Since the object changes slightly over slices subsequently, μ_{O_i} and σ_{O_i} are ML estimates of the statistic properties of pixel intensities of O_{i+1}, encompassed by true B_{i+1}. Let $I(r)$ be the intensity of a pixel r in the processed image, then

$$I'_{i+1}(r) = T(I(r)) = \left(1 + \exp\left(-\frac{I(r) - \mu}{\kappa\sigma_{O_i}}\right)\right)^{-1} \quad (4)$$

Factor κ controls the coverage of the mapping window. The transform process enhance the edge information of the target region using a priori ROI characteristic derived from segmentation of previous slice. $f_{\mathcal{P}}(r)$ is the probability prediction of whether pixel r is located on B_{i+1}. Let $P_i = \{p_k\}$, $k = 1, \cdots, K$, be pixels located on B_i. A_k be the neighborhood of pixel p_k. Let $\mu_{B_i,A,k}$ and $\sigma_{B_i,A,k}$ be the intensity mean and standard deviation of pixels in A_k, which can be cubic, sphere, square, or circle with a radius of R_A. Thus,

$$\mu_{B_i,A} = \frac{1}{K} \sum_{1 \le k \le K} \mu_{A,k}, \quad \sigma_{B_i,A} = \frac{1}{\sqrt{K}} \sum_{1 \le k \le K} \sigma_{A,k} \quad (5)$$

are estimates of the overall sample statistic properties of B_i. Thus, $f_{\mathcal{P}}(r)$, for instance, can be defined as

$$f_{\mathcal{P}}(r) = 1 - (\alpha \left| \frac{\mu_{I_{i+1},A,r} - \mu_{B_i,A}}{\sigma_{B_i,A}} \right| + \beta \left| \frac{\sigma_{I_{i+1},A,r} - \sigma_{B_i,A}}{\sigma_{B_i,A} + \sigma_{I_{i+1},A,max}} \right| + \gamma \left| \frac{\sigma_{B_{i+1},A,r} - \sigma_{B_{i+1},A,p}}{\sigma_{I_{i+1},A,max}} \right|) \quad (6)$$

where $\sigma_{I_{i+1},A,max}$ is the maximal neighborhood standard deviation, calculated as Eq.5, of pixels on image I_i. α, β, and γ are preset parameters. The probability prediction cost can also use statistic features of both interior and exterior regions. $f_{\mathcal{P}}(r)$ reduce cost for pixels located along the boundary.

In order to iteratively adjust the boundary to approach to the true boundary, the number N of control points $S = \{s_j\}$ should be selected corresponding to the size of the B_i and boundary condition, and to seek the optimal boundary. Small N results in lack of control between two subsequent s_j and s_{j+1}, so that the boundary segment between such a pair of seeds might be incorrect, especially when the boundary condition is weak. Large N, on the other hand, limits the searching area, so that it is not able to adjust the boundary candidate iteratively toward the real one while increasing computation. N can be set manually or automatically. Let

$$\zeta_{it}(N, B_{i+1}) = \sum_{1 \le j \le N} \zeta(s_j, s_{j+1}) \quad (7)$$

be the accumulated cost of B_{i+1} at iteration it, where the segment cost is the accumulated cost of each pair of pixels along that segment, $\zeta(s_j, s_{j+1}) = \sum_{1 \le k_j \le K_j} \varsigma(p_{k_j}, p_{k_j+1})$. N candidates can be determined in advance based on size of B_{init} ($K_{B_{init}}$), intensity mean and standard deviation of interior and exterior areas, μ_{int}, μ_{ext}, σ_{int}, and σ_{ext}, such as $N = 2^n$, where

$$n = \frac{K_{B_{init}}}{N_T \bullet \lambda_1 \left| \frac{\mu_{int} - \mu_{ext}}{\mu_{int} + \mu_{ext}} \right| \bullet \lambda_2 \left| \frac{\sigma_{int} - \sigma_{ext}}{\sigma_{int} + \sigma_{ext}} \right|} \quad (8)$$

λ_1 and λ_2 are preset parameters and N_T is a predefined threshold (a integer). Thus, N is small when boundary is strong and large otherwise. Then, an optimal value is chosen by

$$\hat{N} = \arg \min_{N, N \pm \epsilon} \bar{\zeta}^{\Delta}(N, B) \quad (9)$$

where ϵ is a preset perturbation and $\bar{\zeta}^{\Delta}(N, B)$ is the average boundary cost of from slice i to $i + \Delta$ if N, $N - \epsilon$, or $N + \epsilon$ is used. This is to check the impact of such candidate for a range of the continuous slices so that an ideal one can be determined to detect optimal boundary.

III. RESULTS

To evaluate the performance of the proposed approach, we applied it to segment 20 lymph nodes from two high-resolution chest CTs [1], whose voxel spacing are $\{\Delta x = \Delta y = 0.64, \Delta z = 0.5\}$ mm and $\{\Delta x = \Delta y = 0.72, \Delta z = 0.5\}$ mm. Both images were acquired without using contrast agent and reconstructed using a soft kernel. The selected lymph nodes vary in geometric and anatomical features, and are located in prevascular, retrotracheal, lower paratracheal, subaortic (AP window), and para-aortic lymph node stations [8], [9]. Segmentation of those ROIs from an expert is used as ground truth data. The 20 lymph nodes vary in size, shape, and intensity distribution, thus are typical ROIs in lung interventions. Among the 20 lymph nodes, the proposed method was able to segment 18 (9 from each). Accuracy rate calculated as the overlap of a segmentation and the ground truth[2], [5], [4]. Fig. 3 shows several lower paratracheal lymph nodes and corresponding segmentation results using the proposed method. It is quite normal that a lymph node is surrounded by other lymph nodes or anatomical soft-tissue structures.

Table I gives a summary of the segmentation results derived from the segmentation approach. Overall, the approach provides robust and accurate the 3D segmentation performance. We also applied the method to segment 5 liver tumors that are more challenging than lymph nodes above. Table II gives a summary of the segmentation accuracy by comparing the results with corresponding ground truth data, which are manual segmentation from an expert. Fig.4 shows example segmentation results regarding a tumor candidate adjacent to the azygos vein, a tumor in the middle of liver and close to the chest wall, and a tumor area after ablation treatment.

IV. CONCLUSION

ROI segmentation is important to disease detection, diagnosis, treatment, and follow-ups, such as lung and liver cancer. The task is quite challenging because of the limitation of CT image in presenting such soft-tissue structures, and geometric and anatomical difficulties relevant to the ROIs. This paper presents a semi-automatic approach that improves the performance of our previous 3D extension of live wire in ROI segmentation from CT images. We evaluated this method by applying it on both lymph nodes and difficult

liver ROIs. The results show the robustness and efficacy of the proposed approach.

V. ACKNOWLEDGEMENT

Dr. William E. Higgins, Distinguished Professor in Electrical Engineering, Penn State University, provided the CT chest images for lymph node segmentation. Thomas Tang and Lyubomir Zagorchev, Philips Healthcare and Research, N.A., provided CT data for liver ROI segmentation.

Lymph Node	Scan 1 (%)	Scan 2 (%)
1	91	89
2	90	88
3	80	83
4	83	90
5	93	91
6	88	86
7	81	75
μ	87	86

Table I. Accuracy of lymph-node segmentation using the proposed method.

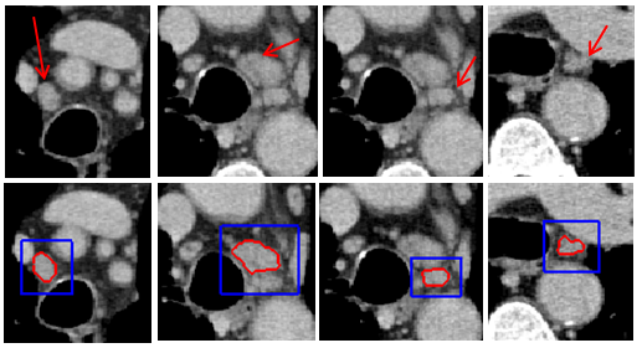

Fig. 3. Example lymph nodes that were segmented by the proposed method. The first row shows lymph nodes, pointed by red arrows, in original images. The second shows corresponding sample segmentation results.

ROI	1	2	3	4	5	Average
Accuracy	93	90	88	91	94	91.2

Table II. Accuracy of liver ROI segmentation using the proposed method.

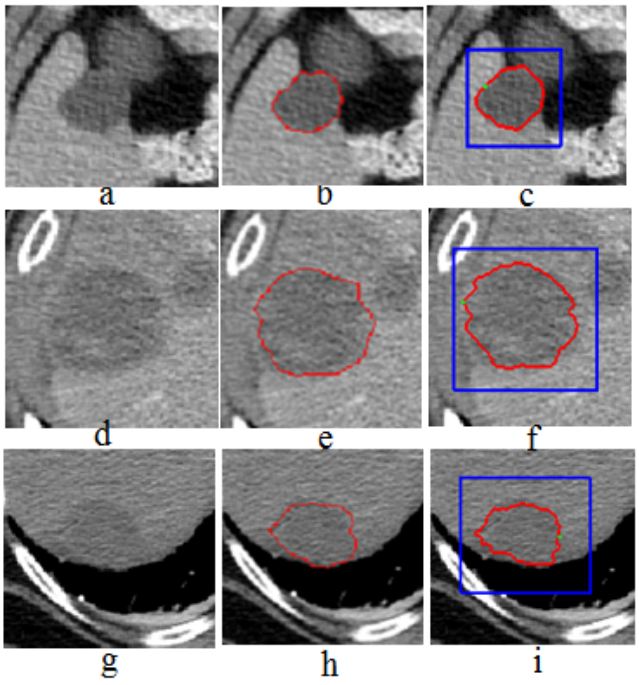

Fig. 4. Example liver ROIs that were segmented by IILW and SSLW. (a,d,g). Original images of a tumor that is adjacent to azygos vein, a tumor in the middle part of the liver while close to chest wall, and a tumor area after ablation, respectively. (b,e,h) are ground truth given by the expert. (c,f,i). Example segmentation results from the proposed method shown in 2D axial slices.

VI. REFERENCES

[1] K. Lu and W.E. Higgins, "Segmentation of the central-chest lymph nodes in 3D MDCT images," *Computers in Biology and Medicine*, vol. 41, no. 9, pp. 780–789, Sept. 2011.

[2] A. X. Falcão, J. K. Udupa, S. Samarasekera, and S. Sharma, "User-steered image segmentation paradigms: Live wire and live lane," *Graphical Models and Image Processing*, vol. 60, no. 4, pp. 233–260, July 1998.

[3] E. N. Mortensen and W. A. Barrett, "Interactive segmentation with intelligent scissors," *Graphical Models and Image Processing*, vol. 60, no. 5, pp. 349–384, Sept. 1998.

[4] K. Lu and W. E. Higgins, "Interactive segmentation based on the live wire for 3D CT chest image analysis," *International Journal of Computer Assisted Radiology and Surgery*, vol. 2, no. 3-4, pp. 151–167, Dec. 2007.

[5] A. X. Falcão and J. K. Udupa, "A 3D generalization of user-steered live-wire segmentation," *Medical Image Analysis*, vol. 4, no. 4, pp. 389–402, Dec. 2000.

[6] A. Schenk, G. Prause, and H.-O. Peitgen, "Efficient semiautomatic segmentation of 3D objects in medical images," in *MICCAI'00: Proc. of the Third International Conference on Medical Image Computing and Computer-Assisted Intervention*, London, UK, 2000, pp. 186–195, Springer-Verlag.

[7] G. Hamarneh, J. Yang, C. McIntosh, and M. Langille, "3D live-wire-based semi-automatic segmentation of medical images," in *SPIE Medical Imaging 2005: Image Processing*, J. M. Fitzpatrick and J. M. Reinhardt, Eds., Apr. 2005, vol. 5747, pp. 1597–1603.

[8] J. Ko and M. Betke, "Chest CT: automated nodule detection and assessment of change over time – preliminary experience," *Radiology*, vol. 218, no. 1, pp. 267–273, Jan. 2001.

[9] K. Lu, P. Taeprasartsit, R. Bascom, R.P. Mahraj, and W.E. Higgins, "Automatic definition of the central-chest lymph-node stations," *Int J Comput Assist Radiol Surg*, vol. 6, no. 4, pp. 539–555, July 2011.